THE PENNSYLVANIA STATE UNIVERSITY
SCHREYER HONORS COLLEGE

DEPARTMENT OF ENGINEERING SCIENCE & MECHANICS

State Space Structure & Global Stability of Hof Inverted Pendulum Walking Models

WILLIAM CORVINO
SPRING 2024

A thesis
submitted in partial fulfillment
of the requirements
for baccalaureate degrees
in Aerospace Engineering and Engineering Science
with honors in Engineering Science

Reviewed and approved* by the following:

Joseph Cusumano
Professor of Engineering Science & Mechanics
Thesis Supervisor & Honors Advisor

Lucas Passmore
Professor of Engineering Science & Mechanics
Faculty Reader

*Signatures are on file in the Schreyer Honors College.

Abstract

This thesis focuses primarily on understanding the structure of Hof inverted pendulum walking models, analyzing both the state space structure and the stability properties. We assert that walking models require mechanics, a controller, and constraints; and without all three, the model is not complete. Under this premise, we generate the concept of recovery basins, derived from viability/global stability of these complete models. In generating these basins, we recover a potential reason for a stability strategy called basin-shifting: changing walking parameters or controllers to keep one's center of mass state within the recovery/viability basin.

Table of Contents

List of Figures **iii**

Acknowledgements **v**

1 Introduction **1**

1.1 Literature Review 2

2 The Inverted Pendulum Walking Model **6**

2.1 The Inverted Spherical Pendulum 7

2.2 Step Transition Maps 9

2.3 Heel-Strike Transition 10

3 Local & Global Stability Analysis **13**

3.1 Fixed Points & Local Stability 14

3.2 Global Stability: Recovery Basins 18

3.2.1 Recovery Basin for Constant Offset 19

3.2.2 Recovery Basin for Positional Control 22

4 Discussion **28**

Bibliography **31**

List of Figures

1.1 Compass walker with swing-leg dynamics. In [1], the compass walker is placed on a ramp of angle γ. The feet in this model have mass m, while the remainder of the mass is concentrated at the center of mass. Stance leg refers to the leg that is planted during the step, while the swing leg rotates about the center of mass throughout the step. This figure is derivative of [1]. 3

1.2 Inverted pendulum model. Center of pressure (COP) is used as a proxy for foot placement. Note that the true inverted pendulum has length l and originates at the center of pressure (rather than the heel) and connects to the center of mass (COM) [2]. 4

2.1 Inverted spherical pendulum with mass m, length L, displacement from vertical θ, and heading ϕ. Note that in this formulation, x is the forward/sagittal direction and z is the lateral/frontal direction. 8

2.2 The coordinate system used in this formulation to account for the alternation of stance feet. The direction of the z measurement flips during each step transition, so that COM locations between the step positions are always positive. The origin of the coordinate system also shifts during each step transition, shifting between the step positions. The figure shows the various measurements as derived from each coordinate frame with the "+/-" superscripts, as previously described. 11

3.1 Unstable trajectory generated from the constant step width/length controller. Done for a constant step width of 0.1 m, step length of 0.5 m, 0.5 s step time, and natural frequency 4.952 Hz for 15 steps. The initial conditions for the simulation were the fixed point defined in Equation (3.1) to within machine precision. Note that the trajectory diverges from the periodic trajectory after about 13 steps. 15

3.2 Results of MATLAB simulation of the constant offset model. (a) A bundle of stable trajectories centered around the fixed point given in Equation (3.5). The simulation was done with target step width 0.1m, target step length 0.5m, step time 0.5s, and natural frequency 4.952Hz. These simulations also display the inertial semistability of the constant offset controller, since it does not have any bias towards a particular final inertial position, unlike the proportional controller. (b) MATLAB simulation demonstrating that the constant offset controller can produce biodynamically unviable trajectories while remaining stable. In this simulation, the walker takes a large backwards crossover step. 16

3.3 Results of MATLAB simulation of the absolute positional error proportional controller. Note that this controller only applies in the lateral direction, so the sagittal direction is controlled by the constant offset controller. (a) A bundle of stable trajectories centered around the fixed point given in Equation (3.9). The simulation was done with target step width 0.1m, target step length 0.5m, step time 0.5s, natural frequency 4.952Hz, and controller gain k = 0.101. These simulations converge very quickly to one trajectory. (b) A bundle of unstable trajectories. These were generated using the same methods and parameters as the stable trajectories, but use a k value of 0.193. While these trajectories remain centered around the target z position, the total width of the trajectory increases step-over-step. 17

3.4 Numerical (dotted) and analytical (smooth) eigenvalues for the absolute positional error proportional controller for variable controller gains. The simulations were done using target step width 0.1m, and varied over the nondimensional time variable ωT. The pink curve represents the non-zero eigenvalue that is independent of k, while the other curves show the gain-dependence of the third eigenvalue. 18

3.5 The recovery basin for the constant offset controller. The boundaries were generated by evaluating the state numerically using the Poincaré map defined in Equation (2.18b) and checking the kinematic conditions, and then overlaying the analytical boundaries from Equation (3.25). The numerical and analytical boundaries line up exactly in this simulation. 21

3.6 The recovery basin for the absolute positional error proportional controller. The boundaries were generated by evaluating the state numerically using the Poincaré map defined in Equation (2.22) and checking the kinematic conditions, and then overlaying the analytical boundaries from the procedure laid out above. The numerical and analytical boundaries line up exactly in this simulation. Note that the axes in this figure are z_c and $z_n + \frac{1}{\omega}\dot{z}_n$ to allow for the figure to be represented in two dimensions, as a slice of the full three-dimensional recovery basin. 27

Acknowledgements

I wanted to thank Dr. Cusumano for taking a chance on me, fresh out of my first year at Penn State, and for continuing to support me throughout this project and in my academics. I feel fortunate to have been able to work with him on this project and to have had the opportunity to learn from him both through my research and coursework. I would also like to thank Dr. Passmore for taking the time and effort to be on my committee. Finally, I would like to thank Eleanor Corvino for her contribution to several figures.

Chapter 1

Introduction

Walking. We all do it. Every day, we take thousands of steps without even thinking about it, and most of them are taken without falling. But, how do we do this supposedly easy task? This research aims to answer that question primarily through physics-based modeling.

The principle behind simple, physics-based walking models is that walking is simply falling into steps, and that doing so continuously generates the overall gait. The particular model in use in this thesis, the so-called inverted pendulum model, leans heavily into this concept. The main portion of the model only describes the motion between each step (i.e. falling into the next step), while choosing step locations is left to be determined from the goals and constraints.

In this sense, we assert that walking models are not just simply the mechanics behind the center of mass motion, but also the control inputs and biomechanical constraints. In many models, control is often asserted directly on the center of mass; in our formulation, we control the center of mass indirectly by choosing steps, since that is how people affect their walking trajectories. Without biological constraints, a walking model can perform maneuvers that are, while mathematically valid, simply physically impossible. Thus, the imposing of constraints permits our walking model to better match human walking properties.

In this thesis, we study the local and global stability properties of one of these hybrid walker-controller-constraint systems. In doing so, we create recovery basins, regions in the stepping plane in which the walker can return to a stable steady gait. These basins are derived from the concept of viability, incorporating the limitations imposed by the controller and constraints. These recovery basins are limited to a particular controller and set of constraints, and as such provide insight into complex strategies and behaviors exhibited by real walkers.

1.1 Literature Review

Why do we care about walking models? People generally know how to walk. Our interest is not only in understanding the nature of walking, but also to learn about the mechanisms by which we can prevent falling. Inherently, walking is just a sequence of steps which humans fall into, catching themselves repeatedly. Falling occurs when, for whatever reason, be it a mental, perceptual, or physical disturbance, a person cannot catch themselves. This issue is particularly pertinent to the elderly, 3 million of whom are treated for fall-related injuries per year, according to the CDC [3]. Another study found that, in 2015, medical costs from fall-related injuries costed $50 billion [4]. Research on fall prevention could alleviate these massive costs, 75% of which were covered by taxpayers through Medicare and Medicaid [4]. Another important application of this research is physical therapy. Often, patients with leg and spinal cord injuries exhibit odd gait patterns that are difficult to assess [5]. Data-based models can be used to predict the projected improvement in walking ability and can be used to discern some characteristics of the gaits used. However, this work serves as a foundation for understanding the *physics* behind these gaits, which is essential for charting a path towards improved methods of physical therapy.

Even within this field, there are many perspectives from which to approach the development of walking models. One approach to this is data-based predictive modeling, where data taken during walking trials is used to build error-correcting optimal control models, that predict where steps

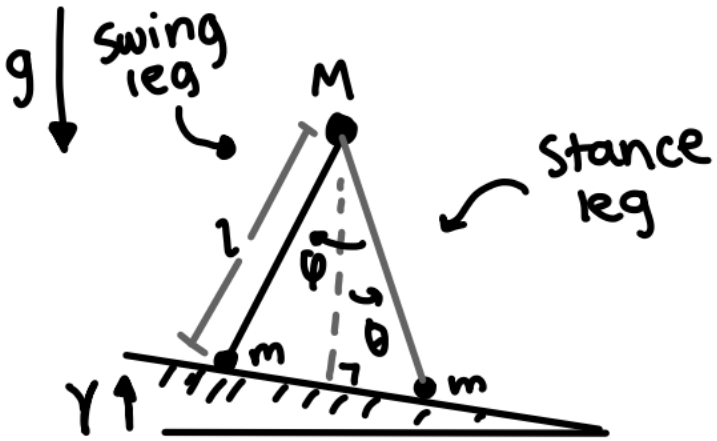

Figure 1.1: Compass walker with swing-leg dynamics. In [1], the compass walker is placed on a ramp of angle γ. The feet in this model have mass m, while the remainder of the mass is concentrated at the center of mass. Stance leg refers to the leg that is planted during the step, while the swing leg rotates about the center of mass throughout the step. This figure is derivative of [1].

will be taken [6]. The advantage of this approach is that it aims to quantify observables and determine the underlying mechanisms through experimentation, without the need to build a new model from first principles. These methods also have the inherent advantage of predicting system behavior, without needing to be reductive for the sake of mathematical and computational tractability. Because of this, the data-driven approach is widely used in the study of gait biodynamics.

However, the approach taken in this analysis is primarily physics-based simple models derived from physics principles, also called templates [7], only intended to capture certain aspects of the biological system they represent. While they are not complete, they can provide valuable insight into the underlying properties of the system and allow for more thorough mathematical, due to their lower dimensionality and mathematical simplicity. That is, the purpose of template models is not necessarily to precisely model every degree of freedom in a system (i.e., a walking person), but to reduce the order of the problem to a degree where the principles of mechanics can inform the analysis.

The most common of these models for walking dynamics are the inverted pendulum (IP) and related models, such as the compass walker. The compass walker is often referred to as the simplest dynamic walker [1, 8, 9, 10, 11]. In its simplest form, it is uncontrolled and, hence, provides an example of *passive dynamic walking*. As seen in Figure 1.1, this model captures the most basic feature of walking walking: falling into each step. Many analyses of this model occur with the model being placed on a descending slope/descending staircase [8] or with an impulse applied at each step [9], both of which allow the walker to be propelled forwards. The model has masses at each foot and at the center of mass (COM), and massless "legs" connecting the feet to the center of mass.

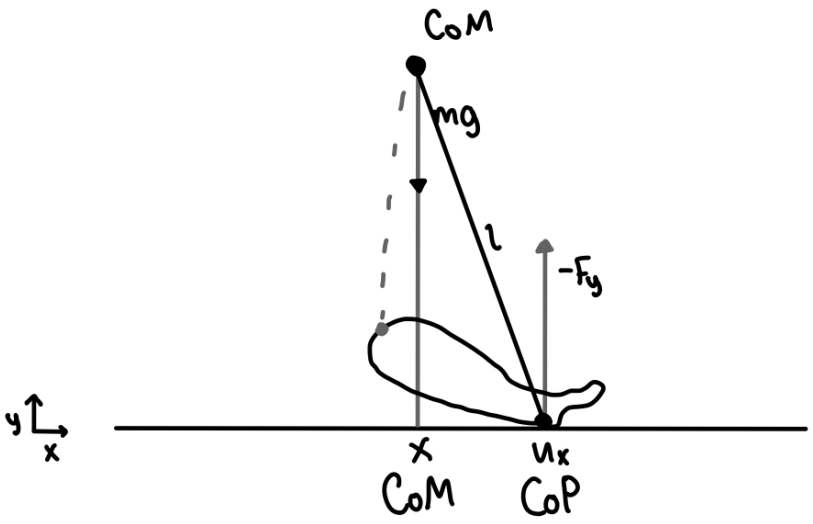

Figure 1.2: Inverted pendulum model. Center of pressure (COP) is used as a proxy for foot placement. Note that the true inverted pendulum has length l and originates at the center of pressure (rather than the heel) and connects to the center of mass (COM) [2].

The inverted pendulum (IP) model, shown in Figure 1.2, is the simplest workable leg model, which gives ample room for analysis and adding complexity. The model consists only of a mass, representing the full mass of the walker concentrated at its COM, connected to a massless center of pressure by a massless link. Swing-leg dynamics are not incorporated in the formulation; instead, the "step" location is given by the center of pressure (COP), which is taken as a control input [2, 12]. Other versions of this model include the spring-loaded inverted pendulum [13], damped bipedal inverted pendulum [14], and linear inverted pendulum plus flywheel [15]. These models contain additional degrees of freedom yielding different levels of biological accuracy at the cost of analytical simplicity.

Many papers studying the compass walker and inverted pendulum models use Poincaré sections and maps [1, 8, 9, 10, 11]. Given the stepping structure of walking, it is useful to study the systems as operating in discrete time. To do this, a snapshot of the state of the system is taken when a certain condition is met during each step cycle. The subspace of the full state space at which these snapshots are taken is called a Poincaré section. When studying the compass walker, the Poincaré section is generally taken at heel strike/step transition [1, 8, 9, 10, 11]; however, it can also be taken elsewhere, such as at midstance. The function relating states between successive snapshots is called a Poincaré map, which is a dynamical model that discretizes the continuous-time gait dynamics. In dynamic walking, the fixed points of these maps are the primary interest, since the fixed points of the discretized system represent periodic gaits in the continuous time system. Local stability of the gait can also be analyzed by linearizing the Poincaré map, through eigenvalue analysis.

Global stability of the models is generally more difficult to capture. In this thesis, as well as in recent literature [9, 12], the concept of *viability* will be used to characterize global stability. A viability region V_n is defined in [12] as "the region in the state space, from which failure can, with appropriate feasible controls, be avoided for at least n steps (one can reach a nonfailed state in n steps) ". The boundaries for failed and non-failed states are generally defined by kinematic and control restrictions. The *viability kernel* V_∞ is the region in which failure never happens, under the same restrictions.

The term "stability" can be ambiguous when discussing gait, since it is often applied both as mathematical stability (as discussed above) and as in the colloquial sense of "remaining upright". To disambiguate the two terms, stability in the mathematical sense will be referred to as "stability" henceforth and stability in the every-day walking sense will be referred to as "fall avoidance".

Ultimately, the goals of this thesis are twofold. First, we aim to clarify the state space of the inverted pendulum class of walking models. The standard state space formulation used in the gait literature is incorrect, as it only considers the motion of the COM between steps [2], which is unstable. While it is technically correct as an analysis of the autonomous inverted pendulum, we argue that the IP model is naturally nonautonomous. The most basic inverted pendulum formulations take the center of pressure (COP; a proxy for foot placement) to be constant during each step, only changing at the moment of heel-strike, when the COP moves instantaneously to the next step location. Even for these models, the nature of the phase space depends on the temporal sequence of COP positions, which is a discrete time-dependent input. Thus, time becomes a state variable which, when combined with the unstable IP phase space, allows for periodic gaits to emerge; if this did not occur, the model's path would always diverge. This discrepancy highlights the importance of clarity when defining the state space, which is arguably the most fundamental concept needed for a mathematical understanding of dynamical systems. Moreover, correcting the state space permits the exploration of variations to the inverted pendulum model, such as analyzing the effects of foot roll during a step and the bipedal stance phase.

The second goal of this thesis is to use viability to analyze the behavior of the inverted pendulum model under the specific controllers originally used in Hof 2008 [2]. We first provide stability analyses (both locally and globally) for this well-known system. In so doing, we gain new insight into dynamic mechanisms relevant to fall avoidance. To do this, kinematic/biological constraints are put on the model as inequalities, and a transgression of these constraints is counted as a "failure", in the sense of Zaytsev's definition [12]. Given the low-dimensionality and linearization of the inverted pendulum model, these restrictions can be evaluated both analytically and numerically. We define *viability basins* that will be generated analytically using the Poincaré maps and mathematical induction; they will be generated numerically using a simulation of the model constructed in MATLAB.

Chapter 2

The Inverted Pendulum Walking Model

2.1 The Inverted Spherical Pendulum

The primary purpose of this chapter is to derive the equations of motion used by Hof [2], and in so doing establish the correct state space structure for the IP model. Hof's IP formulation is a planar pendulum and assumes that the forward and lateral directions can be decoupled when the equations are linearized. We validate this approach by linearizing the equations of motion of an inverted spherical pendulum.

Consider an inverted spherical pendulum of length L and end mass m on a base at position $\mathbf{u}(t)$, as seen in Figure 2.1. The mass m represents the center of mass (COM) of the walker, and $\mathbf{u}(t)$ represents the position of the center of pressure (COP). For the inverted spherical pendulum, define θ as the angle between the pendulum and the vertical, and ϕ as the angle deviation from the forward direction when the pendulum is projected down into the z-x plane. For such a system, the position is defined as

$$\mathbf{r} = \mathbf{L} + \mathbf{u}(t), \tag{2.1}$$

where $\mathbf{r}$ is the position of the mass with respect to the current origin, $\mathbf{L}$ is the position of the mass with respect to the COP, and $\mathbf{u}(t)$ describes the position of the COP with respect to the origin. The vectors $\mathbf{L}$ and $\mathbf{u}(t)$ can be written:

$$\mathbf{L} = L\ (\sin\theta\cos\phi\ \hat{\mathbf{i}} + \cos\theta\ \hat{\mathbf{j}} + \sin\theta\sin\phi\ \hat{\mathbf{k}}). \tag{2.2}$$

$$\mathbf{u}(t) = u_x(t)\hat{\mathbf{i}} + u_z(t)\hat{\mathbf{k}} \tag{2.3}$$

To linearize the model, take the angle θ to be small. Using the first-order Taylor expansion of $\sin\theta$ and $\cos\theta$,

$$\mathbf{L} = L\ (\theta\cos\phi\hat{\mathbf{i}} + \hat{\mathbf{j}} + \theta\sin\phi\hat{\mathbf{k}}) + O(\theta^2), \tag{2.4}$$

which can be simplified by making appropriate trigonometric substitutions:

$$\theta = \sin(\theta) + O(\theta^3) = \frac{\sqrt{x^2+z^2}}{L} + O(\theta^3),$$

$$\cos\phi = \frac{x}{\sqrt{x^2+z^2}},$$

$$\sin\phi = \frac{z}{\sqrt{x^2+z^2}},$$

$$\mathbf{L} = x\hat{\mathbf{i}} + L\hat{\mathbf{j}} + z\hat{\mathbf{k}} + O(\theta^2). \tag{2.5}$$

From this, the acceleration vector can be written by taking two time derivatives, ignoring higher order terms:

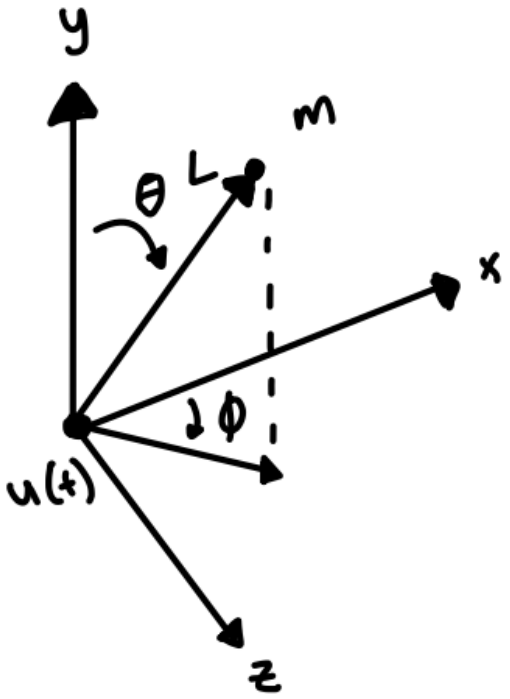

Figure 2.1: Inverted spherical pendulum with mass m, length L, displacement from vertical θ, and heading ϕ. Note that in this formulation, x is the forward/sagittal direction and z is the lateral/frontal direction.

$$\ddot{\mathbf{r}} = \ddot{\mathbf{L}} + \ddot{\mathbf{u}}(t)$$
$$\ddot{\mathbf{r}} = (\ddot{x} + \ddot{u}_x)\hat{\mathbf{i}} + (\ddot{z} + \ddot{u}_z)\hat{\mathbf{k}}. \tag{2.6}$$

Applying Newton's second law:

$$\mathbf{F} = -mg\,\hat{\mathbf{j}} + R\,\hat{\mathbf{L}} = m\ddot{\mathbf{r}}, \tag{2.7}$$

,

where

$$\hat{\mathbf{L}} = \frac{\mathbf{L}}{L},$$

and R is the reaction force from the ground. This can be decomposed into a system of equations in $\ddot{x}$, $\ddot{z}$ and R:

$$m(\ddot{x} + \ddot{u}_x) = R\frac{x}{L}, \tag{2.8a}$$

$$0 = -mg + R, \tag{2.8b}$$

$$m(\ddot{z} + \ddot{u}_z) = R\frac{z}{L}. \tag{2.8c}$$

Solving for $\ddot{x}$ and $\ddot{z}$ yields two linear decoupled ODEs in x & z:

$$\ddot{x} - \frac{g}{L}x = -\ddot{u}_x, \tag{2.9a}$$

$$\ddot{z} - \frac{g}{L}z = -\ddot{u}_z. \tag{2.9b}$$

This is identical to modeling the system as two uncoupled linear inverted planar pendulums, as is done in Hof's original work [2]. Furthermore, these are the same equation in x and z, so their solutions will be the same. In our analysis, the full state space of the system is $(x, \dot{x}, z, \dot{z}; t)$. That is, there are five state variables: the four kinematic states plus time. Time must be included due to the input terms u, which, as will be incorporated in the final model, are necessarily time-varying.

2.2 Step Transition Maps

We now restrict our analysis to the case when the center of pressure $\mathbf{u}$ is constant within each step (i.e. piecewise constant). For this case, Equations (2.9a) can be simplified to a homogeneous equation:

$$\ddot{x} - \omega^2 x = 0, \tag{2.10}$$

where $\omega = \sqrt{\frac{g}{L}}$ is the natural frequency. Despite the input term vanishing, time is not removed entirely as a state variable, since the location of the center of pressure changes at each step. Other COP models may not vanish from the differential equations, but the following analysis can still be done for those cases. Since Equations (2.9a) and (2.9b) are identical and uncoupled, the following analysis is equivalent in both directions. Converting this into a system in the state space $(x, \dot{x})$, this equation becomes:

$$\begin{bmatrix} \dot{x} \\ \ddot{x} \end{bmatrix} = \begin{bmatrix} 0 & 1 \\ \omega^2 & 0 \end{bmatrix} \begin{bmatrix} x \\ \dot{x} \end{bmatrix}. \tag{2.11}$$

The solution to this system is elementary, and can be written in matrix form as:

$$\begin{bmatrix} x \\ \dot{x} \end{bmatrix} = \begin{bmatrix} \cosh(\omega t) & \frac{1}{\omega}\sinh(\omega t) \\ \omega \sinh(\omega t) & \cosh(\omega t) \end{bmatrix} \begin{bmatrix} x_n \\ \dot{x}_n \end{bmatrix}, \tag{2.12}$$

where the subscript n reflects the values for x and $\dot{x}$ at step n; that is, x_n and $\dot{x}_n$ are the initial conditions for the differential equation in each step.

Writing the elapsed time of a step as T, this solution gives the Poincaré map:

$$\begin{bmatrix} x_{n+1} \\ \dot{x}_{n+1} \end{bmatrix}^- = \begin{bmatrix} \cosh(\omega T) & \frac{1}{\omega}\sinh(\omega T) \\ \omega \sinh(\omega T) & \cosh(\omega T) \end{bmatrix} \begin{bmatrix} x_n \\ \dot{x}_n \end{bmatrix}^+, \tag{2.13}$$

in which the subscript "$-$" indicates the state just before heel strike (i.e.at the end of a step) and "$+$" indicates the state just after heel strike, just as in [1]. The corresponding map for the lateral direction is obtained by substituting z for x in Equation (2.13).

2.3 Heel-Strike Transition

The map of Equation (2.13) only takes the step up to just before the next step (i.e. to just before the next heel strike). Thus, to complete the Poincaré map for each step, a heel-strike transition map is needed that will account for the alternation of stance feet. The relationship between the state variables before and after the heel-strike transition makes use of a local, heel-strike-centered reference frame, as shown in Figure 2.2. The inertial reference frame for this analysis will simply be defined as originating at the first COP location, which will be denoted $\mathbf{u}_0$.

These relationships can be described mathematically as:

$$\begin{bmatrix} x_n \\ \dot{x}_n \end{bmatrix}^+ = \begin{bmatrix} x_n \\ \dot{x}_n \end{bmatrix}^- - \begin{bmatrix} u_{xn} \\ 0 \end{bmatrix}^- \tag{2.14a}$$

$$\begin{bmatrix} z_n \\ \dot{z}_n \end{bmatrix}^+ = - \begin{bmatrix} z_n \\ \dot{z}_n \end{bmatrix}^- + \begin{bmatrix} u_{zn} \\ 0 \end{bmatrix}^-. \tag{2.14b}$$

Where u_{xn}^- is a prescribed step length and u_{zn}^- is a prescribed step width, given how the reference frame is constructed. Since the center of pressure at heel-strike is set to be the origin of the reference frame at each step, $\mathbf{u}_n^+ = \mathbf{0}$. This makes the superscripts for $\mathbf{u}$ unnecessary, so they will be omitted in further analysis. This means that the value of $\mathbf{u}_n$ is always measured with respect to the previous COP, $\mathbf{u}_{n-1}$.

Recall that the vector $\mathbf{u}_n$ is an input to the system. In this thesis, we endeavor to analyze the dynamics of the IP model for controllers for $\mathbf{u}$ given in [2].

Consider a control model with constant step length $u_{xn} = L$ and step width $u_{zn} = W$, the heel-strike transition described in Equations (2.14) can be composed with Equation (2.13) to yield the complete step transition map:

$$\begin{bmatrix} x_{n+1} \\ \dot{x}_{n+1} \end{bmatrix}^+ = \begin{bmatrix} \cosh(\omega T) & \frac{1}{\omega}\sinh(\omega T) \\ \omega \sinh(\omega T) & \cosh(\omega T) \end{bmatrix} \begin{bmatrix} x_n \\ \dot{x}_n \end{bmatrix}^+ - \begin{bmatrix} L \\ 0 \end{bmatrix} \tag{2.15a}$$

$$\begin{bmatrix} z_{n+1} \\ \dot{z}_{n+1} \end{bmatrix}^+ = - \begin{bmatrix} \cosh(\omega T) & \frac{1}{\omega}\sinh(\omega T) \\ \omega \sinh(\omega T) & \cosh(\omega T) \end{bmatrix} \begin{bmatrix} z_n \\ \dot{z}_n \end{bmatrix}^+ + \begin{bmatrix} W \\ 0 \end{bmatrix}. \tag{2.15b}$$

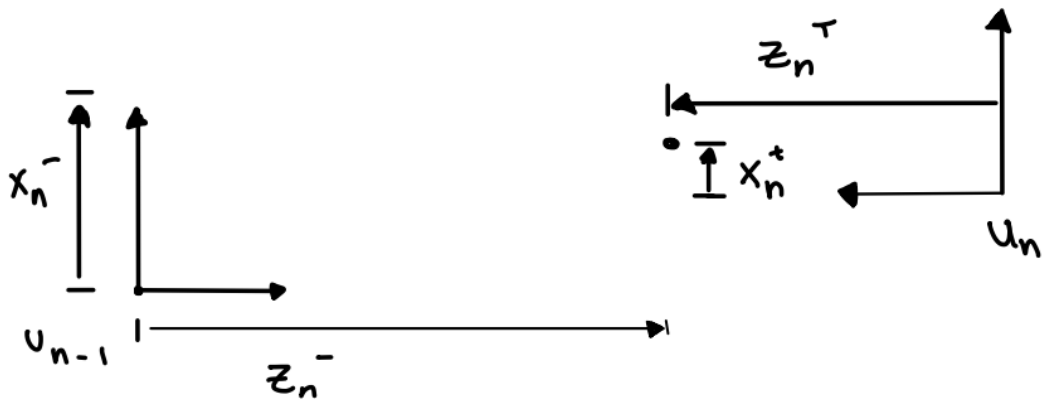

Figure 2.2: The coordinate system used in this formulation to account for the alternation of stance feet. The direction of the z measurement flips during each step transition, so that COM locations between the step positions are always positive. The origin of the coordinate system also shifts during each step transition, shifting between the step positions. The figure shows the various measurements as derived from each coordinate frame with the "+/-" superscripts, as previously described.

Another controller [2] is designed to provide constant step length and width using a "constant offset" The controller has the following form:

$$u_{xn} = x_n^- + \frac{\dot{x}_n^-}{\omega} - b_x \tag{2.16a}$$

$$u_{zn} = z_n^- + \frac{\dot{z}_n^-}{\omega} + b_z, \tag{2.16b}$$

where the constants b are *constant offset values* giving steady-state step length and width:

$$l^* = b_x(e^{\omega T} - 1) \tag{2.17a}$$

$$w^* = b_z(e^{\omega T} + 1). \tag{2.17b}$$

These relationships can be substituted into Equations (2.14) and composed with Equation (2.13) to obtain the step transition map.

$$\begin{bmatrix} x_{n+1} \\ \dot{x}_{n+1} \end{bmatrix}^+ = \begin{bmatrix} -\sinh(\omega T) & -\frac{1}{\omega}\cosh(\omega T) \\ \omega \sinh(\omega T) & \cosh(\omega T) \end{bmatrix} \begin{bmatrix} x_n \\ \dot{x}_n \end{bmatrix}^+ + \begin{bmatrix} b_x \\ 0 \end{bmatrix} \tag{2.18a}$$

$$\begin{bmatrix} z_{n+1} \\ \dot{z}_{n+1} \end{bmatrix}^+ = \begin{bmatrix} \sinh(\omega T) & \frac{1}{\omega}\cosh(\omega T) \\ -\omega \sinh(\omega T) & -\cosh(\omega T) \end{bmatrix} \begin{bmatrix} z_n \\ \dot{z}_n \end{bmatrix}^+ + \begin{bmatrix} b_z \\ 0 \end{bmatrix}. \tag{2.18b}$$

The final controller is similar to the previous, but with absolute positional error proportional control [2]. This controller is only applied in the z-direction, so the analysis of this controller will be restricted to the lateral direction. The step locations are chosen using the following equation:

$$u_{zn} = z_n^- + \frac{\dot{z}_n^-}{\omega} + k(z_n^- + \frac{\dot{z}_n^-}{\omega} - z_{cn}) + b_z, \tag{2.19}$$

where z_{cn} is the z-position target in the heel-strike frame and k is the controller gain. While its value will change at each step, it is important to emphasize that its true position is fixed. That is, the inertial target position is a fixed value, and is denoted z_{c0}. In essence, this means that z_{cn} is how a walking person perceives their target. Since this global value must be converted to the local reference frame at each step, we instead use an update equation:

$$z_{c(n+1)} = u_{zn} - z_{cn} = (k+1)z_n^- + (k+1)\frac{\dot{z}_n^-}{\omega} - (k+1)z_{cn} + b_z. \tag{2.20}$$

Since the map has another parameter that updates after each step, this parameter must be included in the Poincaré map as an additional state variable. The complete step transition map is derived from composing Equation(2.13) with Equations (2.19) and (2.20):

$$\begin{bmatrix} z_{n+1} \\ \dot{z}_{n+1} \\ z_{c(n+1)} \end{bmatrix}^+ = A \begin{bmatrix} z_n \\ \dot{z}_n \\ z_{cn} \end{bmatrix}^+ + \begin{bmatrix} b_z \\ 0 \\ b_z \end{bmatrix}, \tag{2.21}$$

with

$$A = \begin{bmatrix} k\cosh(\omega T) + (k+1)\sinh(\omega T) & \frac{k+1}{\omega}\cosh(\omega T) + \frac{k}{\omega}\sinh(\omega T) & -k \\ -\omega\sinh(\omega T) & -\cosh(\omega T) & 0 \\ (k+1)(\cosh(\omega T) + \sinh(\omega T)) & \frac{k+1}{\omega}(\cosh(\omega T) + \sinh(\omega T)) & -(k+1) \end{bmatrix}. \tag{2.22}$$

As a final remark on the model construction, in Hof's work, and most of the gait biomechanics literature, the IP walking model is not distinguished from an inverted pendulum. The primary difference is the dimensionality of the state space. An inverted pendulum has a two-dimensional state space: $(\theta, \dot{\theta})$ or $(x, \dot{x})$. However, the fact that the COP is a function of time, even in the stepwise constant case, makes time t itself an additional state variable. Thus, for the uncontrolled and constant offset controller, the state space is five-dimensional with state vector $(x, \dot{x}, z, \dot{z}; t)$. In this analysis, we treat this as two independent systems with state space $(x, \dot{x})$ and $(z, \dot{z})$, with the only coupling being time. Furthermore, the positional controller adds another state variable, raising the state space's dimension to six, with state vector $(x, \dot{x}, z, \dot{z}, z_c; t)$. As with the other models, the x and z state variables can be treated independently of each other. The use of Poincaré maps to reduce the continuous-time systems to discrete-time systems then reduces the dimension by one by removing time as a state.

Chapter 3

Local & Global Stability Analysis

3.1 Fixed Points & Local Stability

The local stability of these hybrid walker-controller models is determined using the eigenvalues of the Jacobian of the step transition maps evaluated at their fixed points. They will be evaluated both analytically and numerically using MATLAB simulation. Since all of these maps are written in a local coordinate frame, the analysis here is exclusive to this frame.

First, consider the constant step length/width map presented in Equations (2.15). Combining these into one matrix equation, the fixed point of the map can be computed to be

$$\begin{bmatrix} x^* \\ \dot{x}^* \\ z^* \\ \dot{z}^* \end{bmatrix} = \begin{bmatrix} -\frac{L}{2} \\ \frac{L\omega \sinh(\omega T)}{2\cosh(\omega T)-2} \\ \frac{W}{2} \\ -\frac{W\omega \sinh(\omega T)}{2\cosh(\omega T)+2} \end{bmatrix}. \tag{3.1}$$

Linearizing around this fixed point, we can get the Jacobian of the combined map in Equations (2.15). The characteristic equation of this matrix in the $(x, \dot{x}, z, \dot{z})$ state space is

$$\lambda^4 - 2\cosh(2\omega T)\lambda^2 + 1 = 0, \tag{3.2}$$

which has solutions

$$\lambda_1 = \pm e^{\omega T}. \tag{3.3a}$$

$$\lambda_2 = \pm e^{-\omega T} \tag{3.3b}$$

Since $|\lambda_1| = e^{\omega T} \geq 1$ and $|\lambda_2| = e^{-\omega T} \leq 1$ for $\omega T \geq 0$, this system is an unstable saddle. Furthermore, the magnitudes of the eigenvalues are the same in both the x and z directions. The eigenvectors for both x and z are similarly identical, being equal to:

$$\mathbf{e}_1 = \begin{bmatrix} \frac{1}{\omega} \\ 1 \end{bmatrix} \quad \text{and} \quad \mathbf{e}_2 = \begin{bmatrix} -\frac{1}{\omega} \\ 1 \end{bmatrix}, \tag{3.4}$$

for eigenvalues $\lambda_1 = \pm e^{\omega T}$ and $\lambda_2 = \pm e^{-\omega T}$, respectively. Thus, $\mathbf{e}_1$ is the unstable eigendirection, while $\mathbf{e}_2$ is the stable eigendirection. Since this fixed point is a saddle, the solution moves further from this stable manifold. MATLAB simulations built using this model confirm this instability, as even initial conditions within machine precision of the fixed point diverge in just a few steps. The results of the MATLAB simulation are shown in Figure 3.1.

Similarly, for the constant offset map in Equations (2.18), the fixed point is

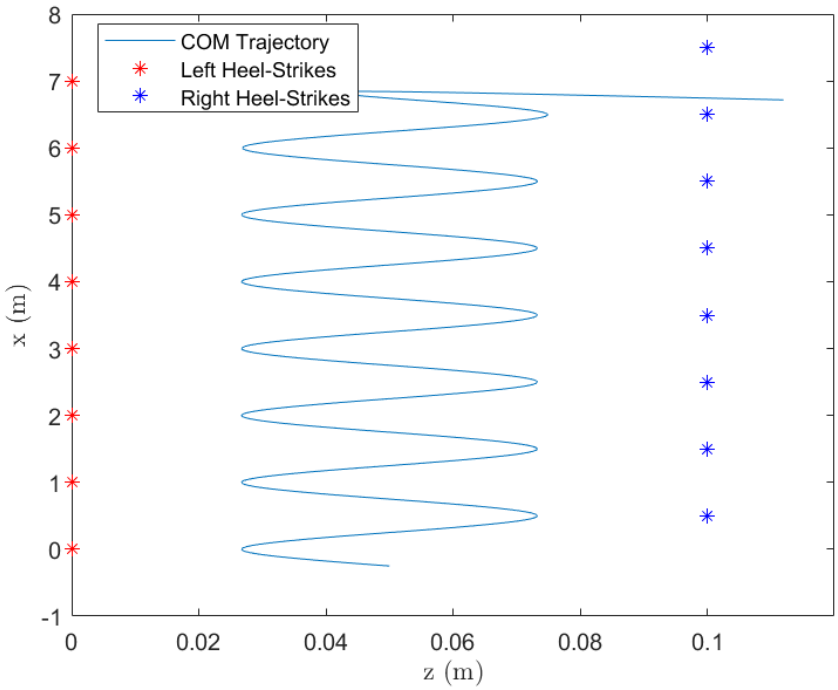

Figure 3.1: Unstable trajectory generated from the constant step width/length controller. Done for a constant step width of 0.1 m, step length of 0.5 m, 0.5 s step time, and natural frequency 4.952 Hz for 15 steps. The initial conditions for the simulation were the fixed point defined in Equation (3.1) to within machine precision. Note that the trajectory diverges from the periodic trajectory after about 13 steps.

$$\begin{bmatrix} x^* \\ \dot{x}^* \\ z^* \\ \dot{z}^* \end{bmatrix} = \frac{1}{2} \begin{bmatrix} -b_x(e^{\omega T} - 1) \\ b_x\omega(e^{\omega T} + 1) \\ b_z(e^{\omega T} + 1) \\ -b_z\omega(e^{\omega T} - 1) \end{bmatrix}. \tag{3.5}$$

This results in a characteristic equation

$$\lambda^4 - e^{-2\omega T}\lambda^2 = 0, \tag{3.6}$$

with solutions

$$\lambda_1 = 0 \tag{3.7a}$$

$$\lambda_2 = \pm e^{-\omega T}. \tag{3.7b}$$

Since $\omega T \geq 0$ implies $\lambda^2 \leq 1$, the constant offset map is stable. Note that, again, the magnitudes of the eigenvalues are equivalent in the x and z directions, but have opposite signs. The eigenvectors for both x and z are

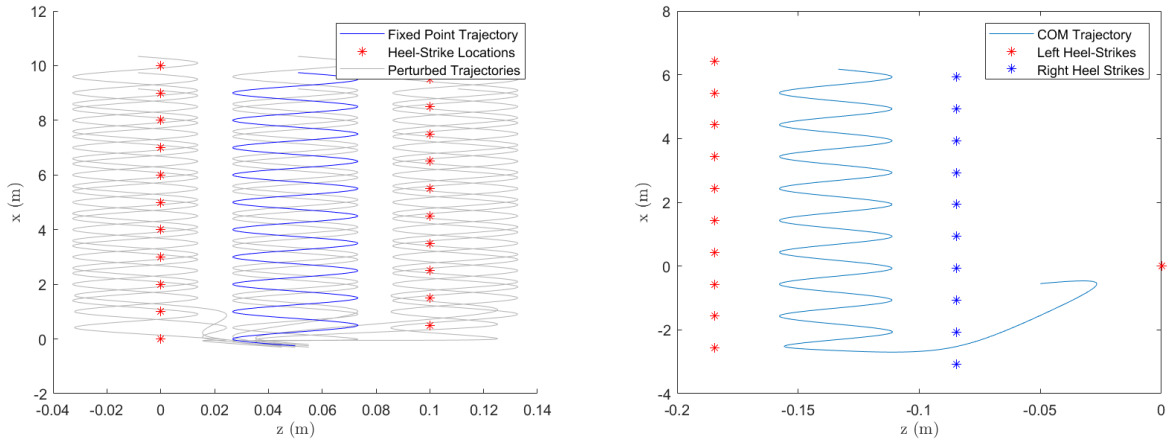

(a) (b)

Figure 3.2: Results of MATLAB simulation of the constant offset model. (a) A bundle of stable trajectories centered around the fixed point given in Equation (3.5). The simulation was done with target step width 0.1m, target step length 0.5m, step time 0.5s, and natural frequency 4.952Hz. These simulations also display the inertial semistability of the constant offset controller, since it does not have any bias towards a particular final inertial position, unlike the proportional controller. (b) MATLAB simulation demonstrating that the constant offset controller can produce biodynamically unviable trajectories while remaining stable. In this simulation, the walker takes a large backwards crossover step.

$$\mathbf{e}_1 = \begin{bmatrix} -\frac{\cosh(\omega T)}{\omega \sinh(\omega T)} \\ 1 \end{bmatrix} \quad \text{and} \quad \mathbf{e}_2 = \begin{bmatrix} -\frac{1}{\omega} \\ 1 \end{bmatrix}, \tag{3.8}$$

for eigenvalues $\lambda_1 = 0$ and $\lambda_2 = \pm e^{-\omega T}$, respectively.

This map always returns stable simulations, even in extreme circumstances. Figure 3.2a shows convergence in a bundle of initial conditions, and Figure 3.2b shows one with "extreme" initial conditions. It should be noted that the simulation in 3.2b takes a step of over two meters in length backwards as a first step. Since this is unlikely to appear in stable gaits, kinematic restrictions are necessary to model realistic walking.

Finally, we evaluate the stability properties of the proportional controller in Equations (2.21) and (2.22). As noted when those equations were derived, only the z-direction will be considered for this controller. The fixed point of this map can be evaluated to

$$\begin{bmatrix} z^* \\ \dot{z}^* \\ z^*_{cn} \end{bmatrix} = \frac{bz}{k - ke^{\omega T} + 2} \begin{bmatrix} e^{\omega T} + 1 \\ -\omega(e^{\omega T} - 1) \\ e^{\omega T} + 1, \end{bmatrix} \tag{3.9}$$

The eigenvalues for this map evaluate to

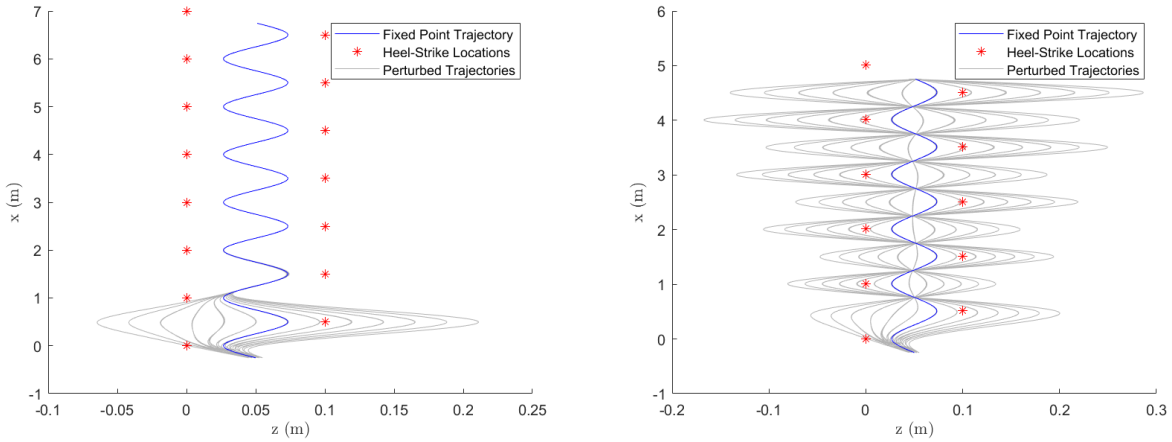

(a) (b)

Figure 3.3: Results of MATLAB simulation of the absolute positional error proportional controller. Note that this controller only applies in the lateral direction, so the sagittal direction is controlled by the constant offset controller. (a) A bundle of stable trajectories centered around the fixed point given in Equation (3.9). The simulation was done with target step width 0.1m, target step length 0.5m, step time 0.5s, natural frequency 4.952Hz, and controller gain k = 0.101. These simulations converge very quickly to one trajectory. (b) A bundle of unstable trajectories. These were generated using the same methods and parameters as the stable trajectories, but use a k value of 0.193. While these trajectories remain centered around the target z position, the total width of the trajectory increases step-over-step.

$$\lambda \in \{0, -e^{-\omega T}, k(e^{\omega T} - 1) - 1\}. \tag{3.10}$$

For this map to be stable, we must have $\lambda_3 = k(e^{\omega T} - 1) - 1 < 1$. Since $e^{\omega T} > 1$ for $\omega T > 0$, we find the following relationship:

$$k < \frac{2}{e^{\omega T} - 1}. \tag{3.11}$$

This provides a maximum gain for stability. As step time T increases, the maximum allowable gain decreases. Again, the simulations confirm this: for small k, the walker converges to a particular target position z_c (see Figure 3.3a), and for large k, the walker's gait width slowly diverges while remaining centered on the target position (see Figure 3.3b).

Simulations were also used to numerically confirm the instability condition in Equation (3.11). For different values of k, the eigenvalues of the system follow exponential curves (which are confirmed numerically, as seen in Figure 3.4). For higher values of k, the allowable normalized step time is small; whereas, for smaller values of k, the range of allowable step times is large.

The eigenvectors for this controller are:

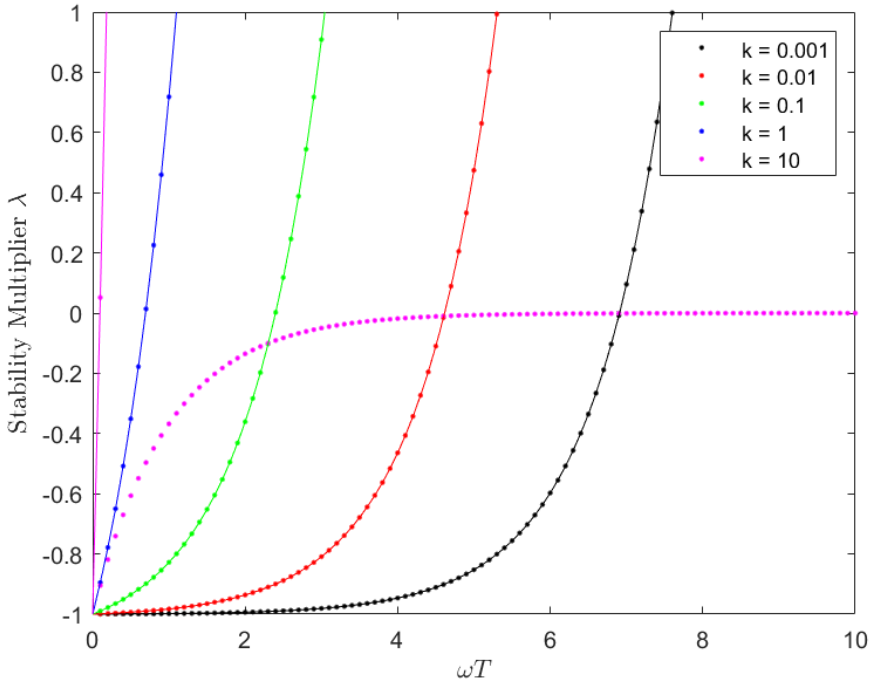

Figure 3.4: Numerical (dotted) and analytical (smooth) eigenvalues for the absolute positional error proportional controller for variable controller gains. The simulations were done using target step width 0.1m, and varied over the nondimensional time variable ωT. The pink curve represents the non-zero eigenvalue that is independent of k, while the other curves show the gain-dependence of the third eigenvalue.

$$\mathbf{e}_1 = \begin{bmatrix} \cosh(\omega T) \\ -\omega \sinh(\omega T) \\ 1 \end{bmatrix}, \quad \mathbf{e}_2 = \begin{bmatrix} -\frac{1}{\omega} \\ 1 \\ 0 \end{bmatrix}, \tag{3.12}$$
$$\text{and} \quad \mathbf{e}_3 = \frac{1}{2(ke^{\omega T}-1)(k+1)} \begin{bmatrix} k(e^{\omega T}+2ke^{\omega T}-1) \\ -k\omega(e^{\omega T}+1) \\ 2(ke^{\omega T}-1)(k+1) \end{bmatrix}.$$

3.2 Global Stability: Recovery Basins

A useful way to describe if a state is stable is to determine if stable walking can be recovered using any available stepping map. The set of all such states, referred to here as a *recovery basin*, can be constructed using the viability kernel V_∞, defined in [12]: starting from any state in V_∞, the walker can take an infinite number of permissible, or "viable" steps.

Our analysis is restricted to locally stable maps. Thus, we take local stability as a *precondition* of viability. Given this precondition, it can be said that a state is viable (i.e. it is contained in V_∞) if

the next step satisfies the kinematic constraints. One such constraint we impose is maximum step width, which can be written as:

$$w = u_{z(n+1)} - u_{zn} < w_{max}. \tag{3.13}$$

Thus, the step width cannot exceed some biomechanical maximum. We also disallow crossover steps which can be written

$$w = u_{z(n+1)} - u_{zn} > 0. \tag{3.14}$$

Note that $u_{zn} = 0$ in our local coordinate system (Figure 2.2), so it is ignored in the analysis. These biomechanical constraints do not account for whether these maps reach a particular state of interest; it only determines if the actions prescribed by the controller violate our predetermined restrictions.

While these recovery basins are defined in a manner similar to viability basins, it is important to note the difference between computing the entire viability kernel and computing the space under just one controller. Recovery basins are viability kernels for the system when any one given controller is applied, and do not determine a system's viability when any control scheme is available. Given the assumption that people have a pool of controllers from which they can pull to achieve different walking gaits, the overall viability kernel for a given person is the union of the recovery basins for all plausible walking controllers.

3.2.1 Recovery Basin for Constant Offset

As an example, consider the recovery basin for the controller described in Equation (2.18b). The step width can be written using Equation (2.16b):

$$w_{n+1} = u_{z(n+1)} = z^-_{n+1} + \frac{\dot{z}^-_{n+1}}{\omega} + b_z = \begin{bmatrix} 1 & \frac{1}{\omega} \end{bmatrix} \mathbf{z}^-_{n+1} + b_z. \tag{3.15}$$

Using Equation (2.13), this can be written in reference to the state at step n:

$$w_{n+1} = \begin{bmatrix} 1 & \frac{1}{\omega} \end{bmatrix} \begin{bmatrix} \cosh(\omega T) & \frac{1}{\omega}\sinh(\omega T) \\ \omega \sinh(\omega T) & \cosh(\omega T) \end{bmatrix} \mathbf{z}^+_n + b_z, \tag{3.16}$$

$$w_{n+1} = e^{\omega T}(z^+_n + \frac{1}{\omega}\dot{z}^+_n) + b_z. \tag{3.17}$$

Applying the inequalities from Equations (3.13) and (3.14), we can obtain a region bound by two parallel lines:

$$0 < w_{n+1} = e^{\omega T}(z^+_n + \frac{1}{\omega}\dot{z}^+_n) + b_z < w_{max}, \tag{3.18}$$

$$-b_z e^{-\omega T} < z_n^+ + \frac{1}{\omega}\dot{z}_n^+ < (w_{max} - b_z)e^{-\omega T}. \tag{3.19}$$

The boundary in Equation (3.19) only gives the region under which the walker is viable after 1 step. This region will be notated R_n^1. This can be generalized to R_n^m, which represents the set of states at step n where the walker will be viable after another m steps (this region is forward invariant through m steps). To expand this to include all steps, consider the following:

1. $R_n^2 = R_n^1 \cap R_{n+1}^1$,
2. $R_n^m = R_n^{m-1} \cap R_{n+1}^{m-1}$,
3. $R_n^m = \bigcap_{i=n}^{n+m-1} R_i^1$.

These properties define a clear procedure for finding the recovery basin. To generate the region at step n where the walker is always viable (viable after an infinite number of steps), Equation (3.19) must be applied at every step $n + m$, then the intersection of the resulting regions defines the recovery basin. For the constant offset map, R_{n+1}^1 can be written as

$$-b_z e^{-\omega T} < z_{n+1}^+ + \frac{1}{\omega}\dot{z}_{n+1}^+ < (w_{max} - b_z)e^{-\omega T}. \tag{3.20}$$

Using Equation (2.18b), we can write:

$$z_{n+1}^+ + \frac{1}{\omega}\dot{z}_{n+1}^+ = \sinh(\omega T)z_n + \cosh(\omega T)\frac{\dot{z}_n}{\omega} + b_z - \sinh(\omega T)z_n - \cosh(\omega T)\frac{\dot{z}_n}{\omega} = b_z, \tag{3.21}$$

so Equation (3.20) becomes

$$-b_z e^{-\omega T} < b_z < (w_{max} - b_z)e^{-\omega T}. \tag{3.22}$$

This result is independent of the step number n, so this defines R_{n+m}^1 for all $m \geq 1$. The left inequality bound is always true; the right bound is true only for certain values of w_{max}:

$$\begin{aligned} b_z &< (w_{max} - b_z)e^{-\omega T} \\ w_{max} &> b_z(e^{\omega T} + 1) = w^*. \end{aligned} \tag{3.23}$$

If this inequality is true, then R_{n+m}^1 is the whole $(z, \dot{z})$ plane. If it is false, then the set is the empty set. This result comes from the construction of the constant offset controller, which determines step width directly from b_z. Thus, this condition is equivalent to stating that the maximum step width must be higher than the controller's set step width as was found previously by Hof [2].

Using this result, we can say that

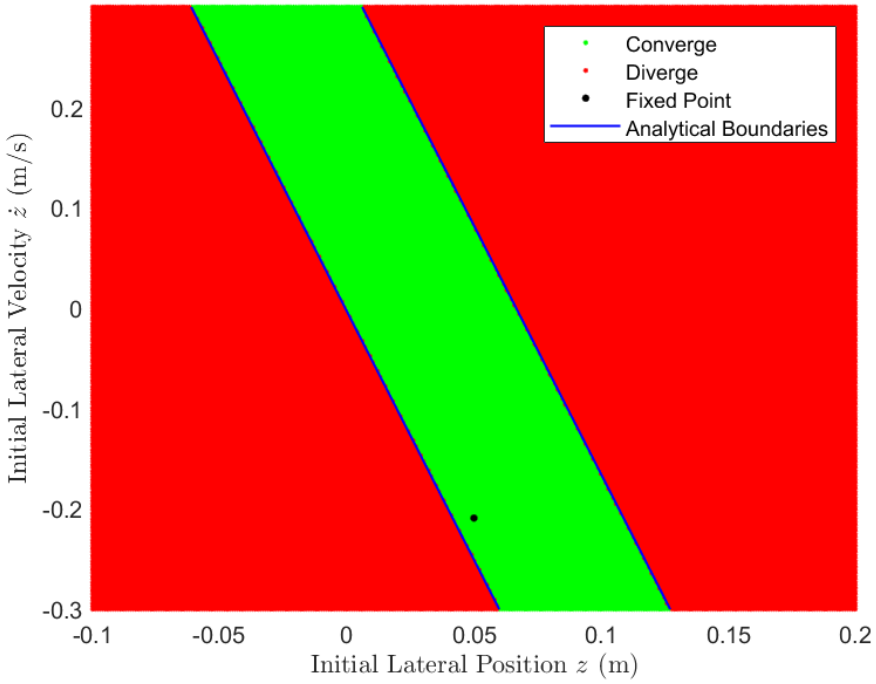

Figure 3.5: The recovery basin for the constant offset controller. The boundaries were generated by evaluating the state numerically using the Poincaré map defined in Equation (2.18b) and checking the kinematic conditions, and then overlaying the analytical boundaries from Equation (3.25). The numerical and analytical boundaries line up exactly in this simulation.

$$R_n^m = \bigcap_{i=n}^{n+m-1} R_i^1 = R_n^1 \cap R_{n+m}^1 = R_n^1 \text{ or } \emptyset. \tag{3.24}$$

Thus, for the constant offset controller, if the walker is viable after one step, it is viable for an infinite number of steps, as long as w_{max} is sufficiently large (via (3.23). Note that if $w_{max} = b_z(e^{\omega T} + 1)$ (its minimum value), R_n^1 can be written

$$-b_z e^{-\omega T} < z_n^+ + \frac{1}{\omega}\dot{z}_n^+ < b_z, \tag{3.25}$$

,

which is thus the limiting case of the smallest possible recovery basin.

Using MATLAB simulations, we verified this theoretical result, as shown in in Figure 3.5, using $\omega = 4.952$ Hz, $T = 0.5$ s, $b_z = 0.0078$ m, and $w_{max} = 0.8$ m.

3.2.2 Recovery Basin for Positional Control

As was done in the previous section, for the absolute positional error proportional controller, we write the step width at the next step as

$$w_{n+1} = u_{z(n+1)} = (k+1)z^-_{n+1} + \frac{k+1}{\omega}\dot{z}^-_{n+1} - kz_{c(n+1)} + b_z, \tag{3.26}$$

$$w_{n+1} = (k+1)e^{\omega T}z^+_n + \frac{k+1}{\omega}e^{\omega T}\dot{z}^+_n - kz_{cn} + b_z. \tag{3.27}$$

From this, we determine the steady-state step width using the fixed points of Equation (3.9):

$$w^* = (k+1)e^{\omega T}z^* + \frac{k+1}{\omega}e^{\omega T}\dot{z}^* - kz^*_c + b_z = 2b_z\frac{e^{\omega T}+1}{2-k(e^{\omega T}-1)} \tag{3.28}$$

Again, this is the same as was found in Hof [2]. Applying the inequalities from Equations (3.13) and (3.14), $0 < w_{n+1} < w_{max}$ becomes

$$0 < (k+1)e^{\omega T}z^+_n + \frac{k+1}{\omega}e^{\omega T}\dot{z}^+_n - kz_{cn} + b_z < w_{max}, \tag{3.29}$$

$$\frac{kz_{cn} - b_z}{(k+1)e^{\omega T}} < z^+_n + \frac{1}{\omega}\dot{z}^+_n < \frac{w_{max} + kz_{cn} - b_z}{(k+1)e^{\omega T}}. \tag{3.30}$$

The region R^1_{n+m} can thus be written as

$$F_m z_{cn} + G_m < z^+_n + \frac{1}{\omega}\dot{z}^+_n < F_m z_{cn} + H_m, \tag{3.31}$$

where we recall that z_{cn} is the additional state variable representing the absolute target position in the current local (body centric) coordinate system. Then F, G, and H, are state-independent coefficients. This creates a new discrete-time dynamical system. Equation (3.30) describes the case for $m = 0$, so we can write

$$F_0 = \frac{k}{k+1}e^{-\omega T}, \tag{3.32a}$$

$$G_0 = \frac{-b_z}{k+1}e^{-\omega T}, \tag{3.32b}$$

$$H_0 = \frac{w_{max} - b_z}{k+1}e^{-\omega T}. \tag{3.32c}$$

Writing R^1_{n+m+1} using Equation (3.30) yields

$$F_m z_{cn+m+1} + G_m < z^+_{n+m+1} + \frac{1}{\omega}\dot{z}^+_{n+m+1} < F_m z_{cn+m+1} + H_m. \tag{3.33}$$

Using Equations (2.21) and (2.22), we can write this at step n as:

$$e^{-\omega T} z_{cn+m} + \frac{(F_m - 1)b_z + G_m}{[k - F_m(k+1)]e^{\omega T}} < z^+_{n+m} + \frac{1}{\omega}\dot{z}^+_{n+m} < e^{-\omega T} z_{cn+m} + \frac{(F_m - 1)b_z + H_m}{[k - F_m(k+1)]e^{\omega T}}. \quad (3.34)$$

Again, identifying the state-independent coefficients, comparing Equations (3.31) and (3.34) yields

$$F_{m+1} = e^{-\omega T}, \quad (3.35a)$$

$$G_{m+1} = \frac{(F_m - 1)b_z + G_m}{D_m}, \quad (3.35b)$$

$$H_{m+1} = \frac{(F_m - 1)b_z + H_m}{D_m}, \quad (3.35c)$$

where for all $m \geq 0$, the denominator term D_m is defined as

$$D_m = [k - F_m(k+1)]e^{\omega T}.$$

Again, the system described in Equations (3.35) are themselves a discrete dynamical system with stability properties. F_m is necessarily stable (since it is constant for $m \geq 1$), but the stability of G and H is less clear.

Since $F^* = e^{-\omega T}$:

$$D^* = [k - F^*(k+1)]e^{\omega T} = k(e^{\omega T} - 1) - 1, \quad (3.36a)$$

$$G^* = H^* = \frac{(F^* - 1)b_z + G^*}{D^*}, \quad (3.36b)$$

which reduces to

$$G^* = H^* = \frac{(e^{-\omega T} - 1)b_z}{D^* - 1} = \frac{e^{-\omega T} - 1}{k(e^{\omega T} - 1) - 2} b_z. \quad (3.37)$$

Since the map is affine, the stability of G and H is determined by the magnitude of the coefficient of G_m and H_m in the update Equations (3.35):

$$|\frac{1}{D^*}| < 1,$$

which reduces to

$$k > \frac{2}{e^{\omega T} - 1} \text{ or } k(e^{\omega T} - 1) < 0. \quad (3.38)$$

The last inequality is always false, given the assumptions that ωT and k are both positive. The left inequality is exactly the reverse of the stability condition in Equation (3.11). So, the G and H maps are stable if and only if the walker is unstable. This could also be intuited using the definition of the recovery basin: if the maps defining the bounds were stable, the recovery basin would shrink towards the fixed point at each step. Since the fixed points of G and H are the same, the recovery basin would collapse to a line.

As with the constant offset map, we are interested in whether the recovery basin R_n^∞ can be determined after a finite number of steps. If so, it will be determined either by the most restrictive basin boundaries or by whether the basin disappears altogether. First, consider the condition for the lower boundary to increase. This can be written as the statement:

$$(F_{m+1} - F_m)z_{cn} + (G_{m+1} - G_m) > 0.$$

Substituting the update equation for G_{m+1}:

$$(F_{m+1} - F_m)z_{cn} + \frac{(F_m - 1)b_z + (1 - D_m)G_m}{D_m} > 0. \tag{3.39}$$

Since F and D only have two "states", this will be evaluated twice: once for $m = 0$ and once for $m \geq 1$. Recalling the definitions of F_0, G_0, and D_m, after some algebra, this inequality for $m = 0$ reduces to

$$z_{cn} > \frac{b_z}{k}\frac{1 + e^{-\omega T}}{1 - e^{-\omega T}}. \tag{3.40}$$

Note that $D_0 = k(e^{\omega T} - 1)$ is always positive. This equation is the condition for the lower boundary to increase after the first step.

A similar analysis can be applied to H_m. The condition for the upper bound to decrease is similar to Equation (3.39):

$$(F_{m+1} - F_m)z_{cn} + \frac{(F_m - 1)b_z + (1 - D_m)H_m}{D_m} < 0. \tag{3.41}$$

Similar to G_m, for $m = 0$, using the definitions of F_0, H_0, and D_0:

$$z_{cn} < \frac{b_z}{k}\frac{1 + e^{-\omega T}}{1 - e^{-\omega T}} + w_{max}(1 - \frac{1}{k(e^{\omega T} - 1)}). \tag{3.42}$$

This is the condition for the upper bound to decrease after the first step.

After the first step (i.e., $m \geq 1$), $F_{m+1} = F_m = F^*$ and $D_m = D^*$, so the inequality in Equation (3.39) reduces to

$$\frac{(F^*-1)b_z+(1-D^*)G_m}{D^*}>0.$$

A similar inequality exists for H_m. It is known that $-1<D^*<1$, but its sign cannot be determined a priori, so consider both the positive and negative cases. For the positive case,

$$G_m>\frac{(F^*-1)b_z}{D^*-1}=G^*. \tag{3.43}$$

This means that, for $D^*>0$ and $m\geq 1$, G_m increases if it is greater than its fixed value, and it can be further determined that G_m always moves in the opposite direction of its fixed point. Alternatively, for $D^*<0$, G_m alternates between being greater than and less than G^*. For the "negative" case, take $G_{m+1}>G^*$ for $m\geq 1$:

$$\begin{aligned}(F^*-1)b_z+G_m<G^*D^*&=\frac{(F^*-1)b_zD^*}{D^*-1},\\ G_m<(F^*-1)b_z(\frac{D^*}{D^*-1}-1)&=G^*.\end{aligned} \tag{3.44}$$

The same result (with flipped inequality) applies for $G_{m+1}<G^*$. We also know that, since the system is unstable, the distance between G_m and G^* will increase after each step. From these cases, we know that the bound due to G_m is the smallest after 1 step. Note that it would not be correct to always call this boundary the lower bound, since H_m may be less than G_m in this alternating case. Since the map is the same for H_m, this result also applies to H.

For this alternating case, since G_m and H_m can no longer approach the fixed point after the first step, it is sufficient to say that the recovery basin is set after i steps, where $i=1$ if either of the following inequalities hold:

$$|G_1-G^*|>|H_2-H^*|=|\frac{H_1-H^*}{D^*}| \tag{3.45a}$$

$$|H_1-H^*|>|G_2-G^*|=|\frac{G_1-G^*}{D^*}|, \tag{3.45b}$$

and is 0 otherwise. This accounts for the possibility that the boundaries switch while making the recovery region smaller. Note that this is true only for the alternating case.

There are a few additional cases of interest. Consider the case where G_m and H_m are both greater than or both less than $G^*=H^*$. Since we know that G_m and H_m both either alternate or stay on the same side of G^* after the first step, we only need to check if they are on the same side after the first step. First, consider the case where $G_1>G^*$ and $H_1>H^*$:

$$G_1=\frac{(F_0-1)b_z+G_0}{D_0}>G^*=b_z\frac{e^{-\omega T}-1}{k(e^{\omega T}-1)-1}.$$

After some algebra, and using the definitions of F_0 and G_0, this reduces to the inequality

$$2 + 2e^{-\omega T} < 0,$$

which is always false. Note that this means that $G_1 < G^*$ in all cases.

Now, consider the other case, where $H_1 < H^*$ and $G_1 < G^*$:

$$H_1 = \frac{(F_0 - 1)b_z + H_0}{D_0} < H^* = b_z \frac{e^{-\omega T} - 1}{k(e^{\omega T} - 1) - 1}. \tag{3.46}$$

Again, after some algebra, this inequality reduces to

$$w_{max} < b_z \frac{2(1 + e^{\omega T})}{2 - k(e^{\omega T} - 1)} = w^*. \tag{3.47}$$

In this case, this means that, if $w_{max} < w^*$, G_m and H_m stay on the same side of H^*. Since both G_m and H_m are unstable, both boundaries increase out to infinity, so the infinite intersection generating R^∞ returns the empty set. It does make sense for the recovery basin to be the null set for a walker that cannot accommodate its own step width.

For completeness, one final case is for either $G_0 > G^*$ or $H_0 < H^*$. $G_0 > G^*$ reduces to

$$k > \frac{e^{\omega T} + 3}{2(e^{\omega T} - 1)} > \frac{2}{e^{\omega T} - 1},$$

which is always false for a stable walking map. For the other inequality:

$$H_0 = \frac{w_{max} - b_z}{k + 1} e^{-\omega T} < H^* = \frac{e^{-\omega T} - 1}{k(e^{\omega T} - 1) - 2} b_z.$$

After some algebra, this reduces to

$$w_{max} < b_z \frac{e^{\omega T} + 1}{2 - k(e^{\omega T} - 1)} = \frac{w^*}{2}.$$

Given the previous condition with w_{max} and step width, this case is redundant.

Having considered all cases, it is sufficient to conclude that, for $D^* > 0$, the most restrictive case always occurs before the second step; that is, $R_n^\infty = R_n^2$. For the alternating case, $R_n^\infty = R_n^{i+2}$, where i is determined by the inequalities in Equations (3.45a) and (3.45b). Since i is always either 0 or 1, it is sufficient to say that $R_n^\infty = R_n^3$ in all cases.

For any individual starting value of z_{cn}, we can generate the boundaries of R_n^∞ using this method. Extrapolating this for all z_{cn}, we get the full recovery basin in the 3D state space. To project this into two dimensions, we will represent it in a z_{cn}-($z_n + \frac{1}{\omega}\dot{z}_n$) plane. We can do this since the slope

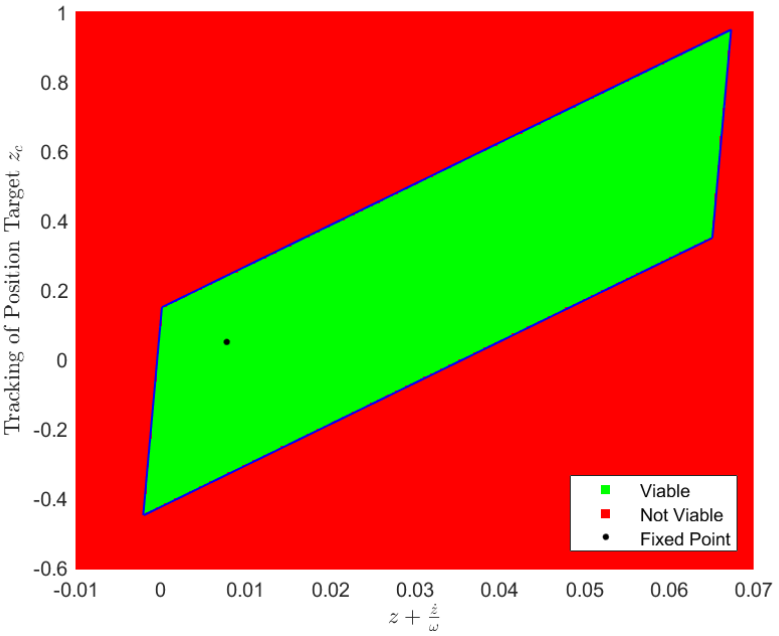

Figure 3.6: The recovery basin for the absolute positional error proportional controller. The boundaries were generated by evaluating the state numerically using the Poincaré map defined in Equation (2.22) and checking the kinematic conditions, and then overlaying the analytical boundaries from the procedure laid out above. The numerical and analytical boundaries line up exactly in this simulation. Note that the axes in this figure are z_c and $z_n + \frac{1}{\omega}\dot{z}_n$ to allow for the figure to be represented in two dimensions, as a slice of the full three-dimensional recovery basin.

of the boundary lines is the same for all values of z_{cn}. The result for an example case is shown in Figure 3.6, generated both using the analytical boundaries as well as evaluating the conditions numerically. Perhaps the most surprising result of generating the recovery basin for the positional error controller is that the tracking of the absolute position target is limited, suggesting that this controller is only viable for targets up to a certain distance away from the current position.

Chapter 4

Discussion

The most fundamental result of this thesis is its description of state space structure. It is important to recognize the true time-dependent nature of the state space of the IP walking model to perform analyses that assess the impact of different control models. This is because the nature of its solutions does not arise from the dynamics of the inverted pendulum itself: that system is unstable, whereas stability of the walking model arises from from the time-dependence of the center of pressure (COP). Even when the COP is held constant within each step, it is not constant *between* steps, shifting positions at each step transition, acting as a "forcing" term even as the equations of motion during each step are homogeneous.

The other primary result of this thesis is the properties of the recovery basins, of which the most notable is the number of steps until convergence. For the constant offset controller, whose recovery basin is described by Equations (3.24) and (3.25), it turns out that the recovery basin, and therefore the global stability properties of the hybrid system, are set after one step. In other words, using this controller, either the walker violates one of our constraints during its first step, or it never does. Similarly, the basin for the absolute positional error proportional controller, the recovery basin converges in only three steps. These results are very similar to those of Zaytsev [16], in which they show that if a given gait is achievable, it is achievable in two steps in most cases. While recovering this with simple controllers may be unsurprising, achieving similar results using a different implementation of viability theory is encouraging.

As in this study, most other discussions of the IP and related models have used a constant center of pressure located at heel strike. However, people roll their feet during their steps, which would make the between-step equations of motion (Equations (2.9)) non-homogeneous. Furthermore, whereas piecewise constant COP models assume that the COP shifts instantaneously between step positions, in reality the COP shifts continuously during mid-stance. Understanding the he time-dependent nature of the system's state space will allow for the implementation of COP controllers that mimic these behaviors using the same model structure developed here.

Another extension of these higher-fidelity COP models is understanding the effects of continuous system noise. It is possible to approximate the solution to a stochastic (noisy) system analytically, e.g. using the Euler-Maruyama method [17, 18], which uses a sum of sinusoids to represent continuous pseudorandom noise. The statistics of the pseudorandom noise could thus generate a probability of walking instability, further evaluating the global stability of given COP controllers.

This thesis focuses solely on controllers developed by Hof [2]; however, the same procedures can be used to analyze other control schemes. For example, a multi-objective optimal controller could be implemented, as was studied in [6]. This would allow us to investigate the relationship between the controller costs and recovery basin boundaries. It is likely that each person weights walking parameters differently (such as step width and walking speed) from each other, from task to task, and throughout their lives. Understanding the effects that these weightings have on the recovery basin, and therefore the global stability of the walker, may be important in understanding the deterioration of fall avoidance in older humans and in analyzing the effects of neuromuscular disorders. A natural continuation of this work would be analyzing the relationship between parameter weights, recovery basin shape, and ultimately fall avoidance. These results are testable as well; it is possible to generate multi-objective control models based on walking data from real subjects, extracting the parameter weights from center of mass and center of pressure data [6]. These models could be used to generate recovery basins from human walking data. Using the model in this way would

provide a metric for global stability that is otherwise impossible to obtain.

Finally, this thesis provides insight into the fall-avoidance strategy known as basin-shifting, previously proposed as a mechanism for fall recovery [9]. The results of the recovery basin for the proportional controller in Figure 3.6 suggest that the recovery basin is limited in the range of target positions that lead to stable walking, a characteristic that this controller likely shares with other simple formulations. This limitation is perhaps not surprising: after all, attempting a large course-correction within a small number of steps is typically not feasible. But, the same effect can be achieved by dividing the larger maneuver into many sub-maneuvers, hence shifting the recovery basin for the controller along the desired trajectory. Note, however, that the specific controllers used may significantly impact the implementation of basin shifting: Hof specifically states that the proposed control laws are intended only to reach a stable gait, and are not designed to match a particular gait [2]. Thus, it is possible that a different controller would be able to accommodate for this limitation by being more conservative or by considering many future steps.

Bibliography

[1] Mariano Garcia, Anindya Chatterjee, Andy Ruina, and Michael Coleman. The simplest walking model: Stability, complexity, and scaling. *Journal of Biomechanical Engineering*, 120(2):281–288, 1998. doi: 10.1115/1.2798313.

[2] At L. Hof. The 'extrapolated center of mass' concept suggests a simple control of balance in walking. *Human Movement Science*, 27(1):112–125, 2008. doi: 10.1016/j.humov.2007.08.003.

[3] Facts about falls. *Centers for Disease Control and Prevention*, May 2023. URL `https://www.cdc.gov/falls/facts.html`.

[4] Curtis S. Florence, Gwen Bergen, Adam Atherly, Elizabeth Burns, Judy Stevens, and Cynthia Drake. Medical costs of fatal and nonfatal falls in older adults. *Journal of the American Geriatrics Society*, 66(4):693–698, 2018. doi: 10.1111/jgs.15304.

[5] Charlotte Werner, Meltem Gönel, Irina Lerch, Armin Curt, and László Demkó. Data-driven characterization of walking after a spinal cord injury using inertial sensors. *Journal of NeuroEngineering and Rehabilitation*, 20(1), 2023. doi: 10.1186/s12984-023-01178-9.

[6] Jonathan B. Dingwell and Joseph P. Cusumano. Humans use multi-objective control to regulate lateral foot placement when walking. *PLOS Computational Biology*, 15(3), 2019. doi: 10.1371/journal.pcbi.1006850.

[7] R. J. Full and D. E. Koditschek. Templates and anchors: Neuromechanical hypotheses of legged locomotion on land. *Journal of Experimental Biology*, 202(23):3325–3332, 1999. doi: 10.1242/jeb.202.23.3325.

[8] Ali Tehrani Safa, Mohammad Ghaffari Saadat, and Mahyar Naraghi. Passive dynamic of the simplest walking model: Replacing ramps with stairs. *Mechanism and Machine Theory*, 42 (10):1314–1325, 2007. doi: 10.1016/j.mechmachtheory.2006.11.001.

[9] Navendu S. Patil, Jonathan B. Dingwell, and Joseph P. Cusumano. Viability, task switching, and fall avoidance of the simplest dynamic walker. *Scientific Reports*, 12(1), 2022. doi: 10.1038/s41598-022-11966-3.

[10] Nelson V. Barnett and Adam C. Lammert. Dynamic stability of passive dynamic walking following unexpected perturbations. *Journal of Biomechanical Engineering*, 145(4), 2022. doi: 10.1115/1.4056166.

[11] Tad McGeer. Passive dynamic walking. *The International Journal of Robotics Research*, 9 (2):62–82, 1990. doi: 10.1177/027836499000900206.

[12] Petr Zaytsev, Wouter Wolfslag, and Andy Ruina. The boundaries of walking stability: Viability and controllability of simple models. *IEEE Transactions on Robotics*, 34(2):336–352, 2018. doi: 10.1109/tro.2017.2782818.

[13] Mustafa Melih Pelit, Junho Chang, Rin Takano, and Masaki Yamakita. Bipedal walking based on improved spring loaded inverted pendulum model with swing leg (slip-sl). *2020 IEEE/ASME International Conference on Advanced Intelligent Mechatronics (AIM)*, 2020. doi: 10.1109/aim43001.2020.9158883.

[14] Bintian Lin, Sigong Zhang, Stana Živanović, Qingwen Zhang, and Feng Fan. Verification of damped bipedal inverted pendulum model against kinematic and kinetic data of human walking on rigid-level ground. *Mechanical Systems and Signal Processing*, 200:110561, 2023. doi: 10.1016/j.ymssp.2023.110561.

[15] Jerry Pratt, John Carff, Sergey Drakunov, and Ambarish Goswami. Capture point: A step toward humanoid push recovery. *2006 6th IEEE-RAS International Conference on Humanoid Robots*, 2006. doi: 10.1109/ichr.2006.321385.

[16] Petr Zaytsev, S. Javad Hasaneini, and Andy Ruina. Two steps is enough: No need to plan far ahead for walking balance. In *2015 IEEE International Conference on Robotics and Automation (ICRA)*, pages 6295–6300, 2015. doi: 10.1109/ICRA.2015.7140083.

[17] Marija Milošević. The euler–maruyama approximation of solutions to stochastic differential equations with piecewise constant arguments. *Journal of Computational and Applied Mathematics*, 298:1–12, 2016. ISSN 0377-0427. doi: https://doi.org/10.1016/j.cam.2015.11.019. URL https://www.sciencedirect.com/science/article/pii/S0377042715005646.

[18] Sunday Fadugba, Bolu Adegboyegun, and O.T. Ogunbiyi. On the convergence of the euler-maruyama method and milstein scheme for the solution of stochastic differential equations. *Int. J. Appl. Math. Model*, 1:9–15, 01 2013.